Front. Phys., 2012, 7(6): 690–700
DOI 10.1007/s11467-012-0259-7

REVIEW ARTICLE

Recent progress on laser-induced breakdown spectroscopy for the monitoring of coal quality and unburned carbon in fly ash

Lei Zhang (张雷), **Zhi-Yu Hu** (胡志裕), **Wang-Bao Yin** (尹王保)†, **Dan Huang** (黄丹), **Wei-Guang Ma** (马维光), **Lei Dong** (董磊), **Hong-Peng Wu** (武红鹏), **Zhi-Xin Li** (李志新), **Lian-Tuan Xiao** (肖连团), **Suo-Tang Jia** (贾锁堂)

State Key Laboratory of Quantum Optics and Quantum Optics Devices, Laser Spectroscopy Laboratory, Shanxi University, Taiyuan 030006, China

E-mail: †ywb65@sxu.edu.cn

Received May 26, 2012; accepted August 29, 2012

Our recent progress on developments of laser-induced breakdown spectroscopy (LIBS) based equipments for on-line monitoring of pulverized coal and unburned carbon (UC) level of fly ash are reviewed. A fully software-controlled LIBS equipment comprising a self-cleaning device for on-line coal quality monitoring in power plants is developed. The system features an automated sampling device, which is capable of elemental (C, Ca, Mg, Ti, Si, H, Al, Fe, S, and organic oxygen) and proximate analysis (Q_{ad} and A_{ad}) through optimal data processing methods. An automated prototype LIBS apparatus has been developed for possible application to power plants for on-line analysis of UC level in fly ash. New data processing methods are proposed to correct spectral interference and matrix effects, with the accuracy for UC level analysis estimated to be 0.26%.

Keywords laser-induced breakdown spectroscopy (LIBS), on-line coal quality analysis, organic oxygen, proximate analysis, unburned carbon, multivariate inverse regression

PACS numbers 42.62.Fi, 52.50.Jm, 89.30.Ag, 42.60.-v

Contents

1 Introduction

In this review, we highlight some of our recent works toward the progress and application of LIBS, including an on-line LIBS coal quality monitoring equipment that apply to coal-fired power plant [1, 2] and an automated prototype LIBS apparatus for on-line analysis of the UC level in fly ash in power plant [3].

The coal quality plays an important role in the whole process of power generation in coal-fired power plant. It is crucial for a power plant control center to change the air/coal mixing ratio and adjust the boiler combustion status according to the current coal quality, especially the elemental distribution and the proximate analysis results (such as the calorific value, ash, and volatile matter, etc.). This demands the installation of suitable on-line analyzers in the power plants for real-time coal quality monitoring. As well as the pre-feedback of coal

* Lei Zhang and Zhi-Yu Hu are co-first authors.

quality analysis, the monitoring of the UC level in fly ash also provides a post-feedback of combustion efficiency at coal-fired power plants. High levels of UC value can have major adverse impacts on combustion efficiency [4] and ash marketing potential.

Current techniques for on-line analysis are based on the methods of X-ray fluorescence spectroscopy (XRF) [5], prompt-gamma neutron activation analysis (PGNAA) [6], near-infrared spectroscopy (NIR) [7], and microwave analysis, etc. Among these analytical techniques, XRF and PGNAA are the most preferable techniques for possible application to power plants and have already been commercially available. However, the XRF technique has difficulties in analyzing light elements such as C and O; the PGNAA technique has limitation for extensive application because of the expensive price, large size, radiation hazard and some other unfavorable factors.

It is thus necessary to develop new techniques suitable for field monitoring. The LIBS technique, which is able to perform simultaneous multi-element analysis of solid [8–10], liquid [11, 12], and gaseous [13–15] substances, is chosen as an effective analytical tool that allows direct chemical analytical of materials by its vaporization achieved by interaction with a laser beam of adequate frequency and intensity, and is suitable to analyze carbon raw material as well as fly ash without any special instrumentation alterations. Therefore, it is an attractive tool for coal-fired power plants [16].

The motivation of this article is to review theoretically and experimentally the characterization of on-line monitoring of coal quality and the UC level in fly ash by use of LIBS. An on-line coal quality monitoring equipment has been designed for a real-time monitoring of the contents of the major elements present in coal (including C, H, Si, Na, Mg, Fe, Ca, Al, Ti, S and organic oxygen), and a mathematic model for transforming the elemental composition into proximate analysis forms has also been established. In addition, a new and versatile apparatus for real-time measurement of UC level in fly ash in coal-fired power plants has been designed.

2 Coal quality analysis

2.1 Elemental analysis of coal

The elemental composition in coal plays a significant role in calculation of the oxygen/coal mixing ratio in boiler combustion. However, it is difficult to obtain the constitution of coal correctly due to its complex structures. To select the optimal data processing methods, samples with absolute concentration are needed. In this work, eight standard powdery coal samples (including low-ash and high-ash coals) were dried prior to analysis. These samples were gathered from the pulverizers of different coal-fired power plants and certified by ICC (Institute of Coal Chemistry, China).

2.1.1 Carbon

Carbon is the most important constituent element of the coal, therefore it is critical to obtain a precise calibration curve of C. In this experiment, with a 1064 nm Q-switched Nd:YAG laser operating at 120 mJ/pulse with 10 Hz as the ablation source, the laser beam is focused on the samples by means of a 10 cm focal length quartz lens to generate the plasma. The focal point is set to 5mm below the surface of the sample, in order to minimize the breakdown of air and aerosols above the sample. A 2 m long all-silica fiber-optic cable is attached to a three channel spectrograph (227–816 nm, 0.3 nm spectral resolution), collecting the plasma emission. A delay of 200 ns and an integration time of 10ms are employed. The rotational speed of the sample cell is 2.7 rev/min. 100 groups of spectrums are collected for analysis and the C (I) 247.9 nm line is selected as the analytical line.

Quantitative analysis methods for C can be summarized as: First, the emission line intensity of C is calculated by removing the background level from the integral intensity of the peak area. The background level can be obtained by averaging intensities of flat regions where the wing of the emission line is; Second, to eliminate the effects of laser energy fluctuation, the measured peak areas are normalized to the total light intensity from the plasma, which can be calculated by summing the intensity of each pixel [17]. The result shows that the relative standard deviation (RSD) of the data reduce nearly 50% after normalized. Finally, the calibration of C element is realized by discarding the negative or zero values, the highest 24% and lowest 17% of the residual data values, averaging the remaining data, and fitting with the carbon content of the samples. The calibration curve from laboratory analysis is shown in Fig. 1, where the correlation coefficient of this non-linear fit and the corresponding standard deviation (SD) value are calculated to be

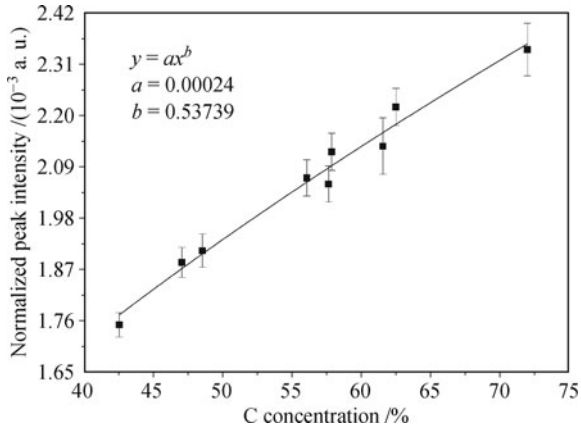

Fig. 1 Calibration curve for C in pulverized coal samples.

0.99% and 1.6%, respectively.

2.1.2 Sulfur

It is difficult to analyze the sulfur content by using LIBS due to its sparse emission lines, the higher excitation potential, and the overlapping of the characteristic lines with other elements'. In addition, the widely used ultraviolet emission lines of sulfur can be quenched easily in air condition [18]. Thus, it is quite important to select the appropriate analytical line and laser energy.

In our experiment, three near-infrared lines of S(I) 921.3 nm, S(I) 922.8 nm, and S(I) 923.8 nm are selected. It is confirmed that the S lines cannot be observed until the laser energy is larger than 160 mJ/pluse. Figure 2 shows a comparison of the spectra of pure pulverized sulfur and two coal samples in the region of 915–935 nm. Here, the S(I) 921.3 nm line is selected as the characteristic analytical line. The calibration curve and error bars for S in coal from laboratory analysis are displayed in Fig. 3, where the correlation coefficient of the linear fit is calculated to be 0.97 and the average SD value is 23.1%. The potential dominant error source in the measurement task is attributed to the spectral interference with the O(I) 926.1 nm line.

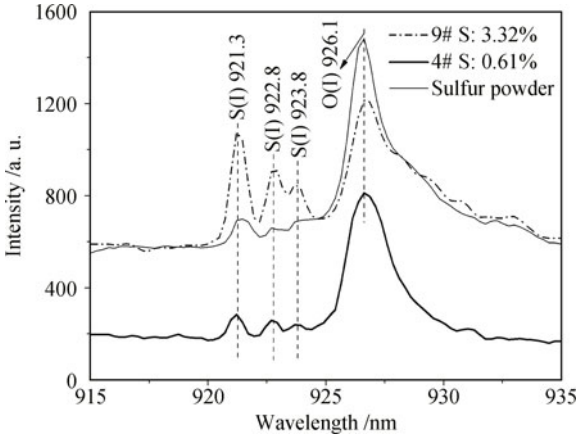

Fig. 2 S line of pure pulverized sulfur and two coal samples.

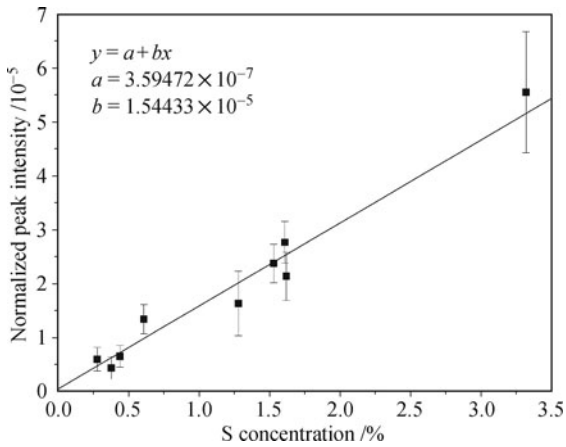

Fig. 3 Calibration curve for S in pulverized coal.

2.1.3 Organic oxygen

Oxygen in dry coal exists in both organic (oxygen containing groups, such as –COOH, –OH, =CO, $-OCH_3$, etc.) and inorganic (oxides dominating the majority) forms [19]. The former is crucial for real-time monitoring to obtain the optimum oxygen/coal mixing ratios for combustion in boilers of coal-fired power plants. Here, we build the calibration formula for organic oxygen (C_{OO}) by subtracting the inorganic oxygen (C_{IO}) content from the total oxygen content (C_{TO}) of coal.

i) Local thermodynamic equilibrium (LTE)

For performing the following procedure to determine the organic oxygen content, it must be demonstrated that the plasma is in the local thermodynamic equilibrium (LTE) condition. Previous reports give the criterion for LTE condition [20, 25]:

$$N_{\mathrm{e}} \geqslant 1.6 \times 10^{12} \times \sqrt{T}(\Delta E)^3 \tag{1}$$

where $N_{\mathrm{e}}(\mathrm{cm}^{-3})$ is the electron density, $T(\mathrm{K})$ is the plasma temperature, and $\Delta E(\mathrm{eV})$ is the largest energy transition. Therefore it is necessary to compute the plasma temperature and the electron density.

Here, the Boltzmann method [25, 26] is used for measuring the plasma temperature. Assuming that the level population obeys the Boltzmann distribution [27], the intensity of a spectral line can be expressed as

$$\ln \frac{I_\lambda^{ki}}{A_{ki} g_k} = -\frac{E_k}{k_{\mathrm{B}} T} + \ln \frac{C_s F}{Z_s(T)} \tag{2}$$

where k_{B} is the Boltzmann constant, λ is the wavelength of the transition, $A_{ki}(\mathrm{s}^{-1})$ is the transition probability, g_k is degeneracy factor, I represents the measured line intensity, C_s is the concentration of the element, $Z_s(T)$ is the partition function, and F is an experimental parameter.

When $\ln[I_\lambda/(gA)]$ is plotted vs. E_k, the slope $-1/(k_{\mathrm{B}}T)$ of this plot is related to the plasma temperature. Here, three spectral lines of O and four of N (specified in Table 1) are selected from the LIBS spectra (see Fig. 4) for measurement. The Boltzmann plots (shown in Fig. 5) yield a temperature of 24600 ± 300 K for N and 26500 ± 300 K for O.

Table 1 The lines and other spectroscopic data used for Boltzmann plot.

Element	Wavelength /nm	E_k /eV	g_k	A_{ki}/s^{-1}
O(I)	777.2	10.74	7	3.69E+07
O(I)	844.6	10.99	5	3.22E+07
O(I)	926.6	12.08	9	4.45E+07
N(I)	746.8	12.00	4	1.96E+07
N(I)	821.6	11.84	6	2.26E+07
N(I)	868.3	11.76	6	1.88E+07
N(I)	904.6	13.73	8	2.80E+07

The electron density is calculated by using the

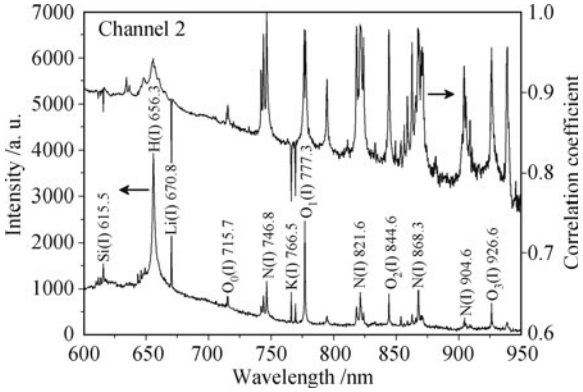

Fig. 4 The averaged spectral correlation between the spectrum and the N(I) line intensity at 746.8 nm (without background subtracted). Reproduced from Ref. [2], Copyright © 2008 Society for Applied Spectroscopy.

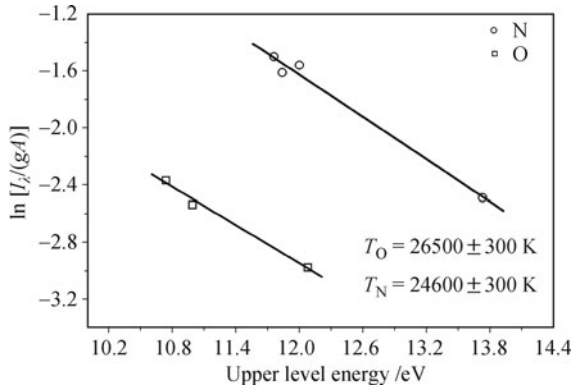

Fig. 5 Boltzmann plots for O(I) and N(I) in the coal sample.

broadening of the spectral line [28]:

$$\Delta\lambda_{\text{stark}} = 2\omega \cdot \frac{N_e}{10^{16}} \tag{3}$$

where ω is the electron impact parameter and N_{e} is the electron number density (cm^{-3}), $\Delta\lambda_{\text{stark}}$ represents the stark broadening (nm), which extracted by fitting a Lorentz profile to the spectral line, the Doppler and pressure broadening are negligible.

Another method for estimating the electron density is calculated from broadening of the H_α line by [29, 30]

$$N_{\text{e}}(\text{cm}^{-3}) = 10^{17}[\text{FWHA(nm)}/0.549]^{1.4713} \tag{4}$$

In our experiments, the electron density calculated by using Eq. (3) for O(I) 777.2 nm, N(I) 746.8 nm, and N(I)868.3 nm is at the order of 10^{17}cm^{-3}; from Eq. (4), we obtain the electron density of $7.657 \times 10^{17}\text{cm}^{-3}$. these results are shown in Fig. 6. With the maximum $\Delta E = 4.2$ eV for N and O, the lower limit of electron number density is $1.9\times10^{16}\text{cm}^{-3}$, therefore the condition of LTE is fulfilled.

ii) Determination of total oxygen content of coal

To yield more accurate results, the internal standard method is applied by calculating the intensity ratio $I_{\text{O}}/I_{\text{N}}$ (I_{O} and I_{N} are the intensities of oxygen and

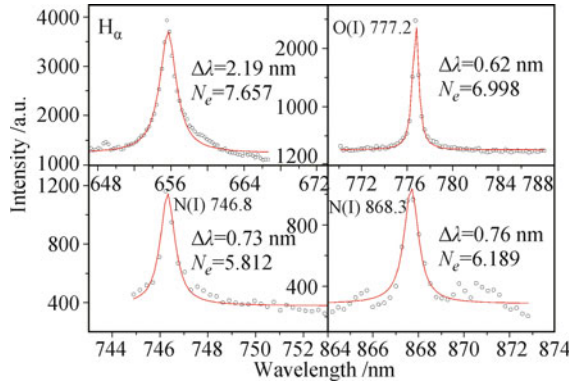

Fig. 6 Lorentz function (*solid line*) fitted to the experimental data points (*circles*) for the H_α-line, O 777.2 nm, N 746.8 nm, and N 868.3 nm, respectively. (N_{e} with the unit of 10^{17} cm^{-3})

nitrogen, respectively). Under local thermal equilibrium (LTE) condition, the intensity ratio $I_{\text{O}}/I_{\text{N}}$ obtained from Boltzmann's law can be expressed as

$$I_{\text{O}}/I_{\text{N}} = \frac{N_{\text{O}} g_{\text{O}} A_{\text{O}} \lambda_{\text{N}}}{N_{\text{N}} g_{\text{N}} A_{\text{N}} \lambda_{\text{O}}} B(T) \tag{5}$$

where

$$B(T) = [Z_{\text{N}}(T)/Z_{\text{O}}(T)] \cdot \exp[-(E_{\text{O}} - E_{\text{N}})/(K_{\text{B}}T)] \tag{6}$$

is a function of plasma temperature T (in K); $Z(T)$ is the partition function for the emitting species; A (in s^{-1}) is the transition probability of the given line; E (in eV) and g are the energies and degeneracies of the upper levels, respectively; K_{B} is the Boltzmann constant; λ (in nm) is the wavelength.

Generally, due to the low concentration of nitrogen in coal ($\leqslant 1$ %), $(N_{\text{N}})_{\text{coal}}$ can be neglected as compared to the nitrogen content in air, and the ratio of amounts of oxygen and nitrogen in air ($(N_{\text{O}})_{\text{air}}/(N_{\text{N}})_{\text{air}}$) are fixed. Then the total oxygen content of coal (C_{TO}) can be deduced as

$$\begin{aligned} \frac{I_{\text{O}}}{I_{\text{N}}} &\propto \frac{N_{\text{O}}}{N_{\text{N}}} = \frac{(N_{\text{O}})_{\text{air}} + (N_{\text{O}})_{\text{coal}}}{(N_{\text{N}})_{\text{air}} + (N_{\text{N}})_{\text{coal}}} \\ &\approx \frac{(N_{\text{O}})_{\text{air}}}{(N_{\text{N}})_{\text{air}}} + \frac{(N_{\text{O}})_{\text{coal}}}{(N_{\text{N}})_{\text{air}}} \propto \frac{(N_{\text{O}})_{\text{coal}}}{(N_{\text{N}})_{\text{air}}} \propto (N_{\text{O}})_{\text{coal}} \propto C_{\text{TO}} \end{aligned} \tag{7}$$

The multi-line analysis method is used to reduce the stochastic errors that depend on the undesired air breakdown, laser energy, spatial mode variations, or irregular surface conditions of the sample. We selected the optimal analytical O(I) lines for calculation of the $I_{\text{O}}/I_{\text{N}}$ ratios by direct study of the correlation between the spectrum and the N(I) line at 746.8 nm, which is previously selected as a reference line (see Fig. 4). For each pixel of the spectrum, the correlation value between the corresponding signal intensity and the N(I) line intensity is obtained through 1500 plasma spectra. Three O(I) lines at 777.2 nm, 844.6 nm and 926.6 nm (marked O_1, O_2, and O_3), were chosen for their correlation coefficient

larger than 0.95. Thus, the "correlation approach" is proposed to yield more accurate I_O/I_N ratios. The Boltzmann method is applied to determining the temperature T, then the function $B(T)$ in Eq. (2) can be calculated using a six-order polynomial with the partition function $Z(T)$ being provided by NIST (see Fig. 7).

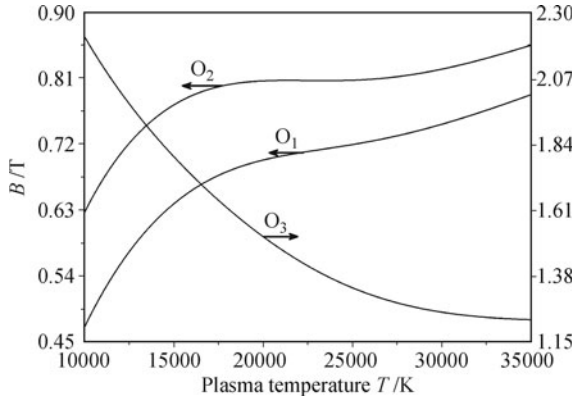

Fig. 7 Simulation of the function $B(T)$ of three O lines at different temperatures. Reproduced from Ref. [2], Copyright © 2008 Society for Applied Spectroscopy.

Finally, we obtain the calibration model of total oxygen written as

$$C_{\mathrm{TO}} = a\sum_{i=1}^{3} b_i \frac{I_{\mathrm{O}_i}}{I_{\mathrm{N}}} + c \tag{8}$$

Eight standard coal samples are used to determine the calibration curve and estimate the coefficients a, b_i, and c, with the result shown in Fig. 8.

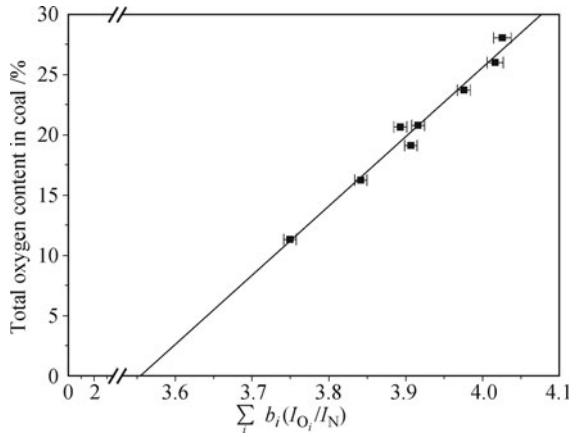

Fig. 8 Calibration curve of total oxygen obtained in laboratory. Reproduced from Ref. [2], Copyright © 2008 Society for Applied Spectroscopy.

iii) Determination of the inorganic oxygen content of coal

For the representative coal in China, SiO_2 and Al_2O_3 together account for 80%–90% of the total inorganic components by weight. As a result, the inorganic oxygen content could be estimated by summing up the corresponding inorganic oxygen contents in SiO_2 and Al_2O_3, the other oxides (Fe_2O_3, P_2O_5, CaO, MgO, TiO_2, etc.) can be neglected. Then the inorganic oxygen content of coal can be expressed as

$$C_{\mathrm{IO}} = 1.14C_{\mathrm{Si}} + 0.89C_{\mathrm{Al}} \tag{9}$$

where the coefficients of 1.14 and 0.89 are obtained from the atomic weight ratios 2O/Si and 3O/2Al, respectively.

Finally, the organic oxygen content of coal can be expressed as

$$C_{\mathrm{OO}} = C_{rmTO} - C_{\mathrm{IO}} \tag{10}$$

Six standard pulverized coal samples are analyzed to validate the feasibility of the calibration formula for organic oxygen, and the result of measurements performed at the plant is shown in Fig. 9. The accuracy is in the range of 1.15%–1.37%.

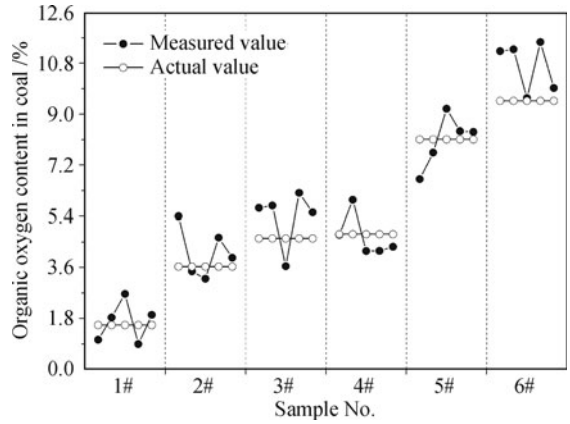

Fig. 9 A comparison between the measured organic oxygen contents and the actual organic oxygen contents through six certified anthracite coal samples according to the on-line apparatus. Reproduced from Ref. [2], Copyright © 2008 Society for Applied Spectroscopy.

2.2 Proximate analysis

For power plants, the expressions for proximate analysis, including fixed carbon (FC_{ad}), moisture (M_{ad}), ash (A_{ad}), volatile matter (V_{ad}), and calorific value (Q_{ad}), are more straightforward than the elemental composition. However, being restricted by the principle of LIBS, the proximate results can only be calculated via the elemental analysis results. At present we have established the transform model of A_{ad} and Q_{ad}.

The procedure for calculating the A_{ad} value is as follows: First, the contents of the main ash-forming elements in coal is determined; subsequently, they are converted into the content of their oxides and then accumulated [31]; Finally, the sum of the oxides is plotted as a function of the A_{ad} value. Here, the main ash-forming elements Si, Al, Fe, Ca, Ti, and Mg are taken into account. Figure 10 shows a linear regressive between the sum of the oxides and the certain A_{ad} value obtained

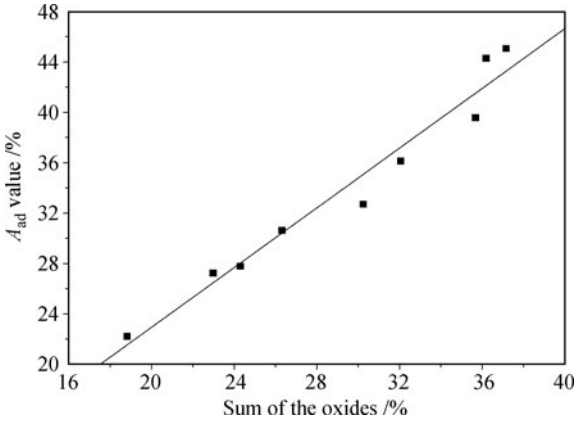

Fig. 10 The relationships between sum of the oxides (SiO_2, Al_2O_3, Fe_2O_3, CaO, TiO_2, and MgO) in coal and the A_{ad} value according to the on-line apparatus.

with nine coal samples, with a correlation coefficient R of 0.98. The corresponding formula can be expressed as

$$A_{ad} = 2.14C_{Si} + 1.89C_{Al} + 1.43C_{Fe} + 1.40C_{Ca} + 1.67C_{Ti} + 1.66C_{Mg} \quad (11)$$

A comparison of the certified and the measured A_{ad} values from the on-line LIBS apparatus performed in the plant is shown in Fig. 11, with relative errors of 7.3%.

The Q_{ad} value is calculated by using the empirical formula [32, 33]:

$$Q_{ad} = 0.3491C_C + 1.1783C_H + 0.1005C_S - 0.0151C_N - 0.1034C_O - 0.0211A_{ad} \quad (12)$$

where C_N value is unavailable for low concentration in coal and high in air, therefore is ignored for its little contribution to the calorific value. By use of the established transformation model, the result obtained from the plant shows that the relative errors are within 11.6% (see Fig. 12).

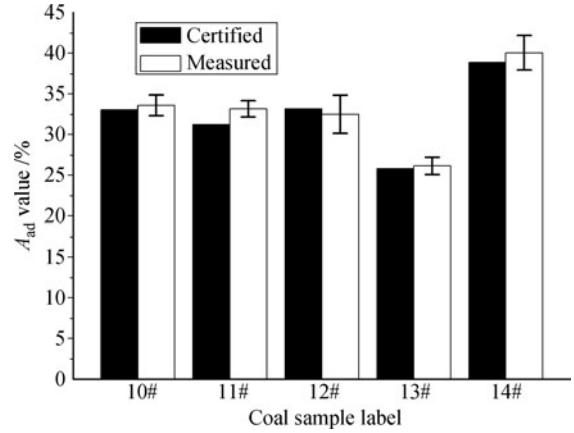

Fig. 11 The calculated A_{ad} values of the five coal samples compared to the certified standards.

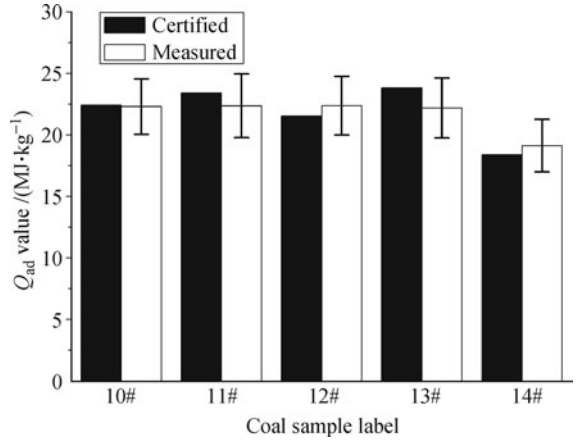

Fig. 12 The calculated Q_{ad} values of the five coal samples compared to the certified standards performed at the plant.

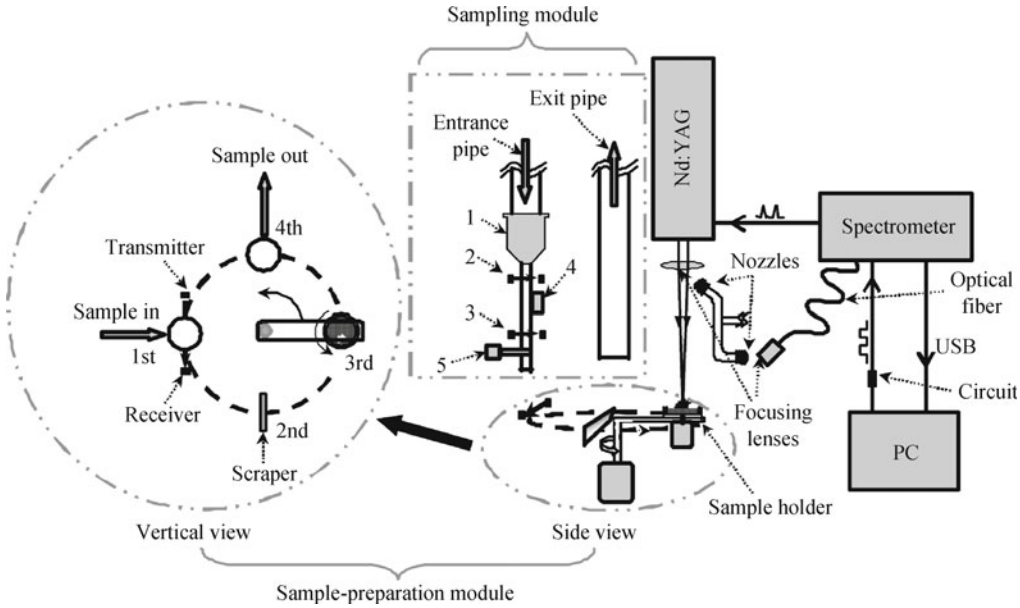

Fig. 13 Schematic representation of the apparatus. The numbers marked in the figure are defined as follows: 1 – Cyclone collector, 2 – The upper optical transmitter-receiver, 3 – The lower optical transmitter-receiver, 4 – Vibrator, and 5 – Unloading valve. Reproduced from Ref. [1], Copyright © 2009 Society for Applied Spectroscopy.

2.3 Analytical apparatus

The entire analysis system consists of an LIBS apparatus and sampling equipment (see Fig. 13). The coal particles come into the cyclone collector with the airflow and fall into the bottom of the entrance pipe. When the predetermined amount of coal is collected, the vibrator and the unloading valve are turned on until all the coal in the entrance pipe has been loaded into the sample holder at the position of "sample in". With the rotation of the axis, the scraper scrapes away the redundant coal particles and smoothes the coal surface in the holder. Then, the holder moves to the laser focus for LIBS analysis. Finally, the residual coal exited through the position of "sample out" and transported back to the coal chute.

Figure 14 shows a photograph of the equipment. The left side of it is the control unit comprising an industrial computer, a spectrometer, and a control box. The right side of the equipment can be divided into three equal portions vertically: on the top there are an exhaust pipe, six branch sampling pipes, and a negative pressure generator; in the middle portion there is a filling pipe, a motor for driving the rotation axis, and the LIBS apparatus will be mounted here; the bottom portion comprises an exit pipe and an electrical distribution system. The equipment is fully software-controlled, and the software is written in visual basic (VB) language.

Fig. 14 Photograph of the equipment for coal quality monitoring.

3 UC level in fly ash

The UC level of fly ash is a key indicator of combustion efficiency at coal-fired power plants. High UC level means incomplete combustion, which would lead to low commercial value. So the UC level can be utilized to optimize the combustion process (including the mill and excess air settings). Here, an apparatus for real-time monitoring of UC level in fly ash in coal-fired power plants based on LIBS has been developed.

3.1 Apparatus

The apparatus consists of an iskinetic sampler, a sample preparation, and an LIBS module (see Fig. 15). The isokinetic sampler with two branch sampling pipes is able to perform interleaved sampling on two flues. Take flue 1 as an example, exhaust gas taken from flue 1 is introduced into the cyclone collector of the sampler firstly. Then the cleansed exhaust gas is discharged through ejector 1 and returns to flue 1, and likewise, the fly ash particles are trapped and dropped down to the bottom of the filling pipe.

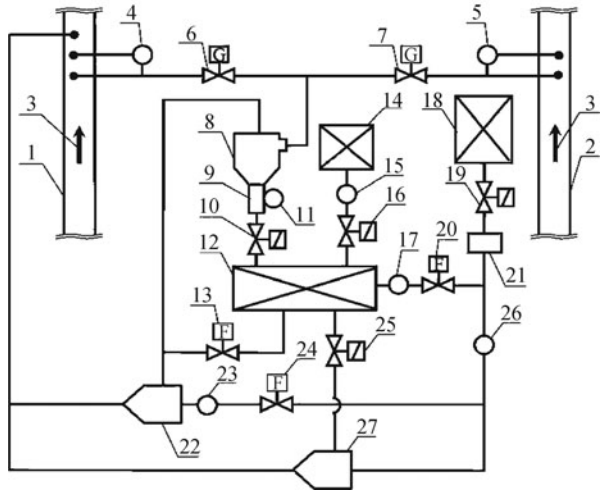

Fig. 15 Schematic of the LIBS apparatus. The numbers marked in the figure are defined as follows: 1 – Flue 1, 2 – Flue 2, 3 – Exhaust gas, 4 – Micro-differential pressure sensor 1, 5 – Micro-differential pressure sensor 2, 6 – Pneumatic valve 1, 7 – Pneumatic valve 2, 8 – Cyclone collector, 9 – Filling pipe, 10 – Solenoid valve 1, 11 – Position sensor, 12 – Sample-preparation module, 13 – Flow-control valve 1, 14 – LIBS module, 15 – Pressure sensor 1, 16 – Solenoid valve 2, 17 – Airflow meter, 18 – Air compressor, 19 – Solenoid valve 3, 20 – Flow-control valve 2, 21 – Freeze drier, 22 – Ejector 1, 23 – Pressure sensor 2, 24 – Flow-control valve 3, 25 – Solenoid valve 4, 26 – Pressure sensor 3, and 27 – Ejector 2. Reproduced from Ref. [3], Copyright © 2011 Society for Applied Spectroscopy.

Only when the amount of ash meets the requirement for analysis, the ash sample is loaded into the sample-preparation module and taken to the measurement point for LIBS analysis. Finally, the residual ash sample is immediately sucked away and transported back into flue 1 via ejector 2.

Figure 16 shows the sample-preparation module and the LIBS module. The ash sample coming from the filling pipe is loaded into the funnel firstly. Then the ash particles pass onto the conveying belt and transported into the center of the chamber where the laser pulse is

focused on for LIBS analysis. Finally, after the measurement, all samples that fell off the belt and accumulated in the bottom shell are taken away from the cleanout door of the shell. Inside the chamber, there are an air inlet port and an air outlet port. The air introduced into the chamber from the inlet path is to dilute the sample gas with air, thus reducing the influence of CO_2 on the measurement of contents of unburned carbon. On the other hand, the continuous gas supply enables the optical lens to avoid accumulating aerosol deposition. The outlet path serves as a dust cleaner for removing the aerosols excited by the powerful laser beams from the location above the laser focus spot quickly so as to reduce the carbonaceous deposition on the optical lens. Moreover, during the LIBS measurement, these aerosols can cause a great attenuation of laser energy via the classical coalitional absorption mechanism as well as a reduction in the fiber collection efficiency. Experimental results reveal that the best flow rates of inlet and outlet port are 0.005 m^3/min and 1.4 m^3/min, respectively.

3.2 Analytical methods

Figure 17(a) shows a typical spectra of fly ash, which reveal most of the components of fly ash such as Zn, Mg, Si, Al, and Ca. Figure 17(b) shows the rectangular region marked "Z" in Fig. 17(a). The C(247.86 nm) line and two Fe lines at 247.98 and 248.33 nm which labeled as Fe_1 and Fe_2 can be seen. However, due to the serious spectral interference, it seems difficult to distinguish the C line from the Fe_1 line. The use of deconvolution can minimize spectral interferences [34], but these emission lines are irregular due to serious peak overlap of C and Fe_1 lines, and are unable to be deconvolved correctly.

A simple formula proposed to estimate the exact C line intensity I_C can be written as

$$I_C = I_{C+Fe_1} - aI_{Fe_2} \tag{13}$$

where I_{C+Fe_1} represents the line intensity contributed by both the C and Fe_1 lines, I_{Fe_2} represents the Fe_2 line intensity, and the coefficient a is a mean intensity ratio of I_{Fe_1}/I_{Fe_2}. The coefficient a can be calculated from a large amount of plasma spectra of pure iron. Here, $a = 0.316$ is obtained in our experiment.

To validate the accuracy of this formula in estimating the C line intensity, an additional high-resolution spectrograph with a narrow spectral range of 243 nm to 254 nm is employed to detect the intensity of C line at 247.9 nm. A comparison of C(247.9 nm) line intensity from this formula and the high-resolution spectrograph of ten ash samples with different carbon content are shown in Fig. 18. The fairly good result confirms the feasibility of this

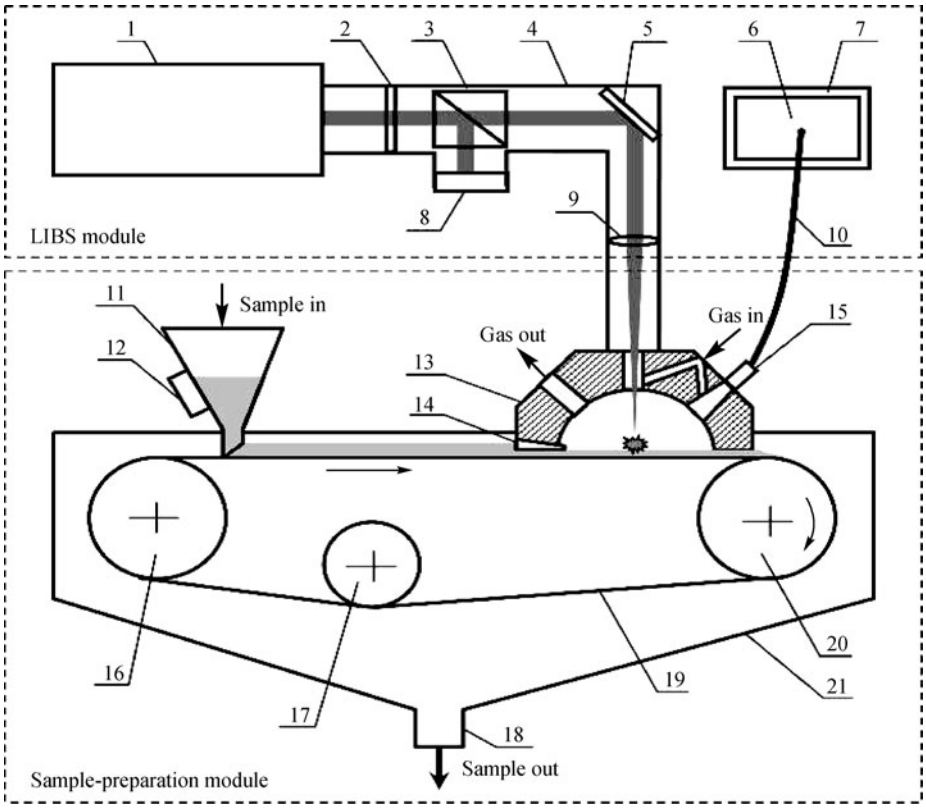

Fig. 16 Schematic of the LIBS module and the sample-preparation module. The numbers marked in the figure are defined as follows: 1 – Nd:YAG laser, 2 – Half-wave plate, 3 – Polarizing beam splitter, 4 – Bolt sleeve, 5 – Rear-silvered mirror, 6 – Spectrometer, 7 – Chiller, 8 – Energy meter, 9 – Focusing lens, 10 – Optical fiber, 11 – Conical funnel, 12 – Vibrator, 13 – A-A section of the connection base, 14 – Smooth groove, 15 – optical fiber splice, 16 – Driven pulley, 17 – Guide pulley, 18 – Cleanout door, 19 – Conveying belt, 20 – Drive pulley, and 21 – Shell. Reproduced from Ref. [3], Copyright © 2011 Society for Applied Spectroscopy.

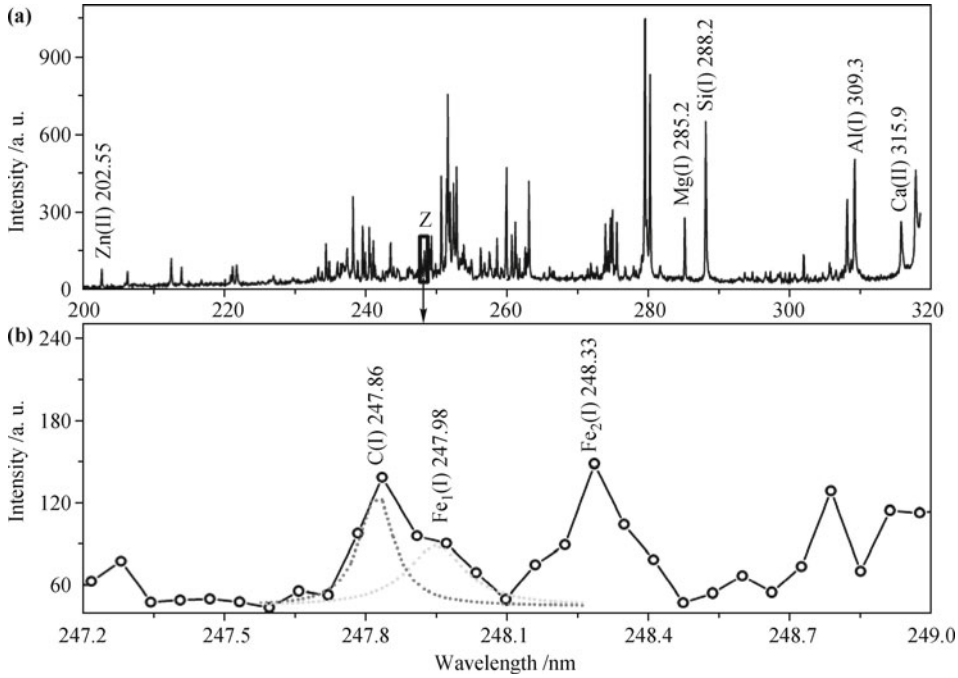

Fig. 17 **(a)** LIBS spectra of fly ash. **(b)** A detailed view of the rectangular region marked with "Z". Specific lines emitted by C and Fe atoms are marked. Reproduced from Ref. [3], Copyright © 2011 Society for Applied Spectroscopy.

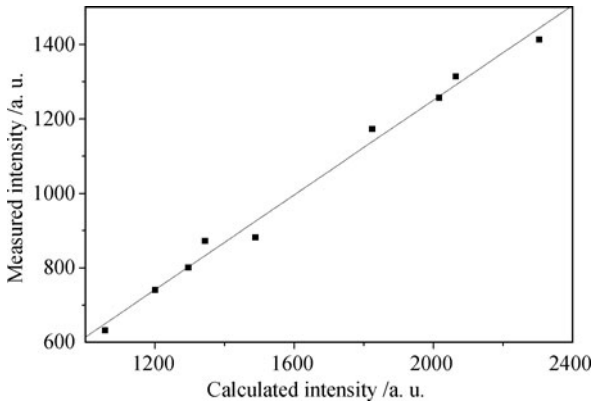

Fig. 18 Comparison of C(247.9 nm) line intensity from the formula and the high-resolution spectrograph of ten ash samples.

formula in estimating the C line intensity. As a result, it negates the requirement of high-resolution spectrograph, which would increase the complexity and cost of the apparatus.

3.3 Calibration model

To build the calibration equation of carbon content C_C in fly ash, nine ash samples (marked 1#–9#) at the same kind of coal and another five samples (marked 10#–14#) from different coal-fired power plants are used in laboratory analysis. According to the traditional calibration model, the intensity of C(247.9 nm) normalized by the intensity of Si(288.2 nm) as a function of the carbon content, the calibration curve is shown in Fig. 19. Here, Si served as the internal standard element owing to its high content and uniform distribution in the ash sample. As can be seen, for 1#–9# ash samples with similar matrices, the curve grows linearly, and there is no evidence of a linear trend for the samples marked 10#–14#. As a result, a revised calibration model must be established to correct the matrix effects [35, 36].

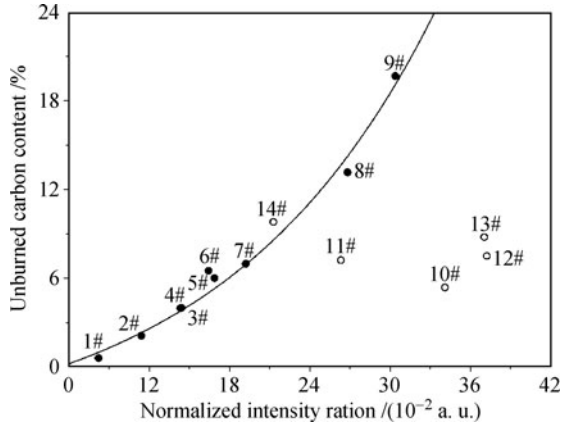

Fig. 19 Traditional calibration curve of C content in fly ash. Reproduced from Ref. [3], Copyright © 2011 Society for Applied Spectroscopy.

To avoid the matrix effects, all the compounds in the sample are taken into account in establishing a reliable calibration model. A second-order polynomial multivariate inverse regression [37, 38] is considered to minimize the matrix effects and guarantee more reliable measurement results. To determine the absolute carbon content C_C in fly ash, the linear multivariate inverse regression method limited to the second-order can be expressed as

$$C_C = a + \sum_i [b_i(\overline{I}_i/\overline{I}_{Si}) + c_i(\overline{I}_i/\overline{I}_{Si})^2] \quad (14)$$

where a, b_i and c_i are the regression coefficients of the nonlinear multivariate regression of element i, $\overline{I}_i/\overline{I}_{\mathrm{Si}}$ is the mean normalized intensity ratio of element i. For most of the ash generated in power plants, the contents of SiO_2, Al_2O_3, Fe_2O_3, CaO, MgO, and ZnO together represent more than 90% of the composition in percentage weight. Therefore, Si(288.2 nm), Al(308.2 nm), Fe(259.9 nm), Ca(315.9 nm), Mg(279.6 nm), and Zn(206.2 nm) are taken into account in the model, and the contribution of other trace-element is ignored. Figure 20 shows the carbon contents measured with this model from laboratory analysis for the corresponding certified values of the calibration samples, an SD value of 0.18% and a correlation coefficient R of 0.997 can be seen.

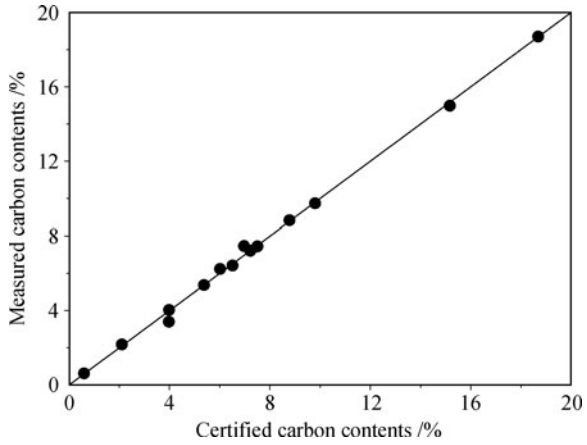

Fig. 20 UC measured with the multivariate regression model for the calibration samples (1#–14#) corresponding certified values. Reproduced from Ref. [3], Copyright © 2011 Society for Applied Spectroscopy.

Another five samples (marked 15#–19#) of different matrices are analyzed to validate the feasibility of the calibration model. Figure 21 shows the comparison of the measured and the certified carbon contents. Based on the quantitative results in laboratory, the measurement accuracy is estimated to be 0.26% while the average relative error is 3.81%.

4 Summary and prospect

In this article, an LIBS system for on-line quality analysis of pulverized coal in power plants has been described. Both elemental (C, Ca, Mg, Ti, Si, H, Al, Fe, S and organic oxygen) and proximate analysis (A_{ad} and Q_{ad}) can be realized, which are capable of performing a pre-feedback to obtain optimal boiler control and to improve the combustion efficiencies of the power plant. Since most power plants prefer the post-feedback by the UC level in fly ash, an LIBS apparatus for on-line characterization of UC level in fly ash is developed with the accuracy estimated to be 0.26%, while the average relative error is 3.81%.

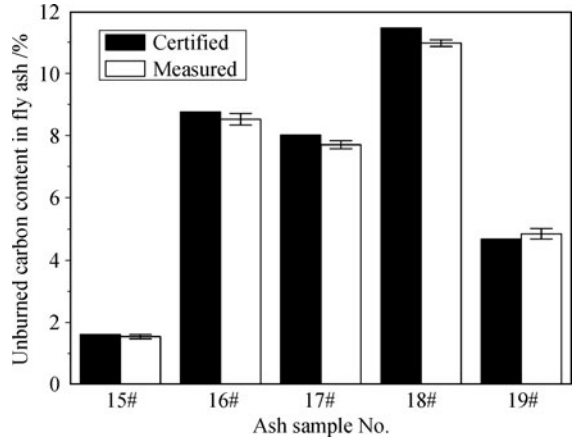

Fig. 21 The calculated unburned carbon contents of the five validation ash samples (15#–19#) compared to the certified standards. Reproduced from Ref. [3], Copyright © 2011 Society for Applied Spectroscopy.

However, it is reported that the coal consumption rises by 0.123g/(kW ·h) while the UC level rises by 0.1% [39]. For example, for a 4 × 300 MW power plant, it will bring

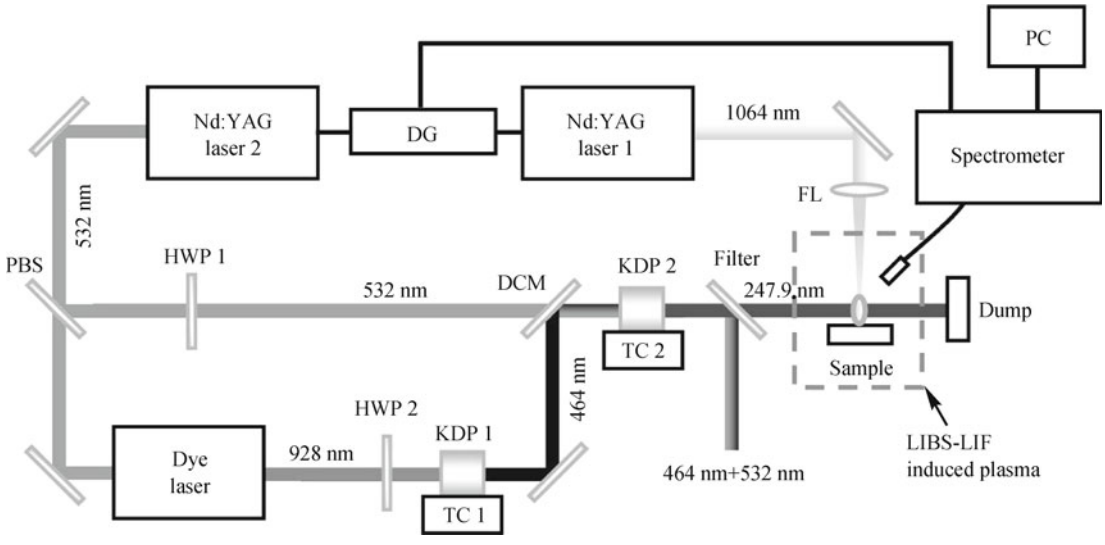

Fig. 22 Experiment scheme of LIBS-LIF.

1300t waste of coal per year, which amounts to a loss of nearly one million RMB. Thus, to further enhance the measurement accuracy can lower the costs significantly. Next work will be devoted to improving the accuracy by utilizing the combined LIBS-LIF technique [40–42].

The LIBS-LIF experimental set-up is shown in Fig. 22. The ablation pulse used is 1064 nm with the energy of approximately 100 mJ and the pulse width of 8 ns. The generated plasma plume is re-excitated by using a 2nd laser pulse with the wavelength being tuned to 247.9 nm in accordance, which populate the C atoms from the $2s^22p^2$ state to the $2s^22p3s$ state. The resonant excitation pulse from nonlinear frequency conversion of dye laser is used to increase the probability of stimulated C atoms and to improve the measurement accuracy.

Acknowledgements This work was supported by the National Natural Science Foundation of China (Grant Nos. 61127017, 61205216, 61275213, 61178009, 61108030, and 60978018), the National Basic Research Program (973 Program) (Grant No. 2012CB921603), International Science & Technology Cooperation Program of China (Grant No. 2001DFA12490), Major Program of the National Natural Science Foundation of China (Grant No. 10934004), NSFC Project for Excellent Research Team (Grant No. 61121064), Environmental Project of Shanxi Province (Grant No. 2011256).

References

1. W. B. Yin, L. Zhang, L. Dong, W. G. Ma, and S. T. Jia, Appl. Spectrosc., 2009, 63(8): 865
2. L. Zhang, L. Dong, H. P. Dou, W. B. Yin, and S. T. Jia, Appl. Spectrosc., 2008, 62(4): 458
3. L. Zhang, W. G. Ma, L. Dong, X. J. Yan, Z. Y. Hu, Z. X. Li, Y. Z. Zhang, L. Wang, W. B. Yin, and S. T. Jia, Appl. Spectrosc., 2011, 65(7): 790
4. K. Styszko-Grochowiak, J. Golaś H. Jankowski, and S. Koziński, Fuel, 2004, 83: 1847
5. J. Marrero, G. Polla, and R. J. Rebagliati, Spectrochim. Acta B, 2007, 62: 101
6. G. Steinhauser, J. H. Sterba, M. Bichler, and H. Huber, Appl. Geochem., 2006, 21(8): 1362
7. A. M. Mouazen, M. R. Maleki, J. De Baerdemaeker, and H. Ramon, Soil Tillage Res., 2007, 93(1): 13
8. C. F. Su, S. Feng, J. P. Singh, F. Y. Yueh, J. T. Rigby, D. L. Monts, and R. L. Cook, Glass Technol., 2000, 41: 16
9. A. I. Whitehouse, J. Young, I. M. Botheroyd, S. Lawson, C. P. Evans, and J. Wright, Spectrochim. Acta B, 2001, 56: 821
10. A. K. Rai, H. Zhang, F. Y. Yueh, J. P. Singh, and A. Weisburg, Spectrochim. Acta B, 2001, 56: 2371
11. G. Arca, A. Ciucci, V. Palleschi, S. Rastelli, and E. Tognoni, Appl. Spectrosc., 1997, 51(8): 1102
12. A. Kumar, F. Y. Yueh, T. Miller, and J. P. Singh, Appl. Opt., 2003, 42(30): 6040
13. D. W. Hahn and M. M. Lunden, Aerosol Sci. Technol., 2002, 33(1–2): 30
14. H. Zhang, F. Y. Yueh, and J. P. Singh, J. Air Waste Manage. Assoc., 2001, 51(5): 681
15. A. W. Miziolek, V. Palleschi, and I. Schechter, Laser-Induced Breakdown Spectroscopy (LIBS): Fundamentals and Applications, Cambridge: Cambridge University Press, 2006
16. M. P. Mateo, G. Nicolas, and A. Yañez, Appl. Surf. Sci., 2007, 254: 868
17. D. Body and B. L. Chadwick, Spectrochim. Acta B, 2001, 56: 725
18. L. Dudragne, P. Adam, and J. Amouroux, Appl. Spectrosc., 1998, 52(10): 1321
19. G. Takeya, Pure Appl. Chem., 1978, 50(9–10): 1099
20. G. Cristoforetti, A. De Giacomo, M. Dell'Aglio, S. Legnaioli, E. Tognoni, V. Palleschi, N. Omenetto, Spectrochim. Acta B, 2010, 65: 86
21. A. W. Miziolek, V. Palleschi, and I. Schechter, editors, Laser-Induced Breakdown Spectroscopy, Cambridge: Cambridge University Press, 2006
22. J. A. Aguilera, C. Aragón, G. Cristoforetti, and E. Tognoni, Spectrochim. Acta B, 2009, 64: 685
23. S. Pandhija and A. K. Rai, Appl. Phys. B, 2009, 94: 545
24. A. Mansoori, B. Roshanzadeh, M. Khalaji, and S. H. Tavassoli, Optics and Lasers in Engineering, 2011, 49: 318
25. M. Sabsabi and P. Cielo, Appl. Spectrosc., 1995, 49(4): 499
26. J. A. Aguilera and C. Aragón, Spectrochim. Acta B, 2007, 62: 378
27. I. Bassiotis, A. Diamantopoulou, A. Giannoudakos, F. Roubani-Kalantzopoulou, and M. Kompitsas, Spectrochim. Acta B, 2001, 56: 671
28. H. R. GRIEM, Plasma Spectroscopy, New York: McGraw-Hill, 1964
29. A. M. El Sherbini, H. Hegazy, and Th. M. El Sherbini, Spectrochim. Acta B, 2006, 61: 532
30. B. Praher, V. Palleschi, R. Viskup, J. Heitz, and J. D. Pedarnig, Spectrochim. Acta B, 2010, 65: 671
31. M. D. Belbot, G. Vourvopoulos, Ph. C. Womble, et al., Conference on Penetrating Radiation Systems and Applications, SPIE, 2000, 3769: 168
32. I. Obernberger and G. Thek, Proceedings of the 1st World Conference on Pallets, 2002, 115
33. S. V. Loo and J. Koppejan (Eds.), Hand Book of Biomass Combustion and Co-firing, Enschede: Twente University Press, 2002
34. D. Body and B. L. Chadwick, Spectrochim. Acta B, 2001, 56: 725
35. D. K. Ottesen and L. L. Baxter, Energ. Fuel., 1991, 5: 304
36. R. Krasniker, V. Bulatov, and I. Schechter, Spectrochim. Acta B, 2001, 56: 609
37. J. Vrenegor, R. Noll, and V. Sturm, Spectrochim. Acta B, 2005, 60: 1083
38. S. Laville, M. Sabsabi, and F. R. Doucet, Spectrochim. Acta B, 2007, 62: 1557
39. L. Y. Zhang and J. T. Xu, Management Engineer, 2010, 5: 46
40. F. H. Kortenbruck, R. Noll, P. Wintjens, H. Falk, and C. Becker, Spectrochim. Acta B, 2001, 56: 933
41. Y. Godwal, S. L. Lui, M. T. Taschuk, Y. Y. Tsui, and R. Fedosejevs, Spectrochim. Acta B, 2007, 62: 1443
42. H. Loudyi, K. Rifai, S. Laville, F. Vidal, and M. Chaker, J. Anal. At. Spectrom., 2009, 24(10): 1421